Effects of Spin-Orbit Interaction Activated Interchannel Coupling on Photoemission Time Delay

Sourav Banerjee,[1] Pranawa C. Deshmukh,[2] Anatoli S. Kheifets,[3] and Steven T. Manson[4]

[1] *Department of Physics, Indian Institute of Technology Madras, Chennai 600036, India*
[2] *Department of Physics, Indian Institute of Technology Tirupati, Tirupati, 517 506, India*
[3] *Research School of Physics, The Australian National University, Canberra ACT 2601, Australia*
[4] *Department of Physics and Astronomy, Georgia State University, Atlanta, 30303, USA*

(Dated: January 19, 2020)

Spin-orbit interaction activated interchannel coupling (SOIAIC) has been investigated theoretically in the time delay domain for $3d$ photoemission in the isoelectronic sequence I^-, Xe and Cs^+ using the relativistic-random-phase approximation with relaxation (RRPA-R). The results show that SOIAIC becomes more important with increasing nuclear charge, and that time delay is affected more strongly than cross sections or photoelectron angular distribution β parameters.

PACS numbers: 32.80.Rm, 32.80.Fb, 42.50.Hz

I. INTRODUCTION

Capturing dynamics of electronic motion within atoms has become reality with an outstanding advancements of ultrafast laser technology. The dynamics of electrons on attosecond time scale can now be resolved using state-of-the-art experimental techniques employing very short laser pulses [1–3]. The fact that the photoionization from atomic systems is not instantaneous and has a time delay associated with it has triggered a large number of studies, both theoretical and experimental [4–24]. These studies were aimed at the determination of the time delay in various situations. The theoretical analysis of the time delay is carried out within the formalism of quantum collision physics developed by Wigner [25], Eisenbud [26], and Smith [27]. Photoionization can be interpreted as a half-collision process, the final state being the same as elastic scattering of an electron from the residual ion. Using this idea, the photoionization time delay is studied in the context of the Wigner-Eisenbud-Smith (WES) time delay. It is defined as the energy derivative of the phase of the complex transition matrix element for the photoemission process. The time delay is an important measurable parameter which provides a sensitive probe of electron correlations and dynamics. In addition, the WES time delay provides direct information about the phase of the matrix element. In the two photon measurement techniques, there are contributions to the total time delay from two different sources: (i) the intrinsic delay $\tau_{\rm WES}$ (i.e., the WES time delay) during the ionization process itself, and (ii) the Coulomb laser coupling contribution, which is due to the interaction of the ionized electron with the combined field of the dressing laser and the residual ionic core. In the present work, we study τ_{WES} which bears the signature of the ionization process. Earlier work has shown that the Wigner-Eisenbud-Smith time delay is very sensitive to electron correlations, especially in the energy region of autoionization resonances [9, 13, 14, 16, 22, 23, 28], near Cooper minima [29], and in the vicinity or inner-shell thresholds [21].

Many-body correlations are at the very foundation of atomic physics and are also responsible for various interesting phenomena. Spin-orbit interaction activated interchannel coupling (SOIAIC) is an example of many-body interactions, specifically the impact of interchannel coupling among the photoemission channels from the two states comprising a spin-orbit doublet. In the present study, we investigate the effect of SOIAIC on the WES time delay spectrum. SOIAIC has been known for some time since its experimental observation [30] in the partial photoionization cross section of Xe $3d$, followed by a theoretical calculation and explanation [31] of the double hump structure in $3d_{5/2}$ cross section. The effect of SOIAIC on various photoionization parameters have also been investigated [32, 33], but there are very few studies [17, 34, 35, 50] dealing with the effects of the spin-orbit interaction on the time delay spectrum. In the present study, we have investigated the photoemission time delay from the spin-orbit split $3d$ subshells of Xe, I^- and Cs^+ which are isoelectronic to one another, to focus upon how time delay varies along the isoelectronic sequence. Previous studies [36] have shown that cross section results using RRPA-R (relativistic random phase approximation with relaxation) [37] were in very good agreement with experiment; therefore, the same has been used in the present study. The RRPA-R formalism takes into account the relativistic corrections and many electron correlations along with the relaxation of the core. The methodology is discussed in the next section.

Note that the variation in the energy-dependent phase involved in photoionization transition channels affects not only the WES time delay but the angular distribution of the photoelectrons as well. The asymmetry β parameter generally shows a significant energy dependence which brings out some, but not all, the physics inherent to the energy-dependent phases. Since β is a ratio [38, 39], some information due to cancellation in the numerator and the denominator is lost. Photoemission time delay, however, captures all of the phase information, being the energy derivative of the complex transition am-

plitude. When the outgoing photoelectron has access to multiple final states in the continuum, interference between these channels leads to spectacular, measurable, angular dependence of the time delay [15, 34, 40]. In this study, energy dependence of the partial photoionization/photodetachment cross sections and the angular distribution asymmetry parameter for photoelectron ejection from the $3d$ subshells of Xe, I^- and Cs^+ is reported. In addition, the energy and angle dependence of the photoionization/photodetachment Wigner-Eisenbud-Smith time delay for these cases are discussed.

II. THEORETICAL METHOD

A. Time delay calculation

The formalism of the angular dependent photoionization/photodetachment time delay has been described earlier [15, 34]. The electric dipole matrix element for a transition from an initial state $a \equiv (l, j, m)$ to the final state $\bar{a} \equiv (\bar{l}, \bar{j}, \bar{m})$ due to the interaction with linearly polarized photons (having its polarization direction along the z-axis) is expressed to within a real multiplicative factor as

$$\begin{aligned} T_{10}^{(1\nu)} &= \sum_{\bar{\kappa}\bar{m}} (\chi_\nu^\dagger \Omega_{\bar{\kappa}\bar{m}}(\hat{p}))(-1)^{\bar{j}-\bar{m}} \begin{pmatrix} \bar{j} & 1 & j \\ -\bar{m} & 0 & m \end{pmatrix} \\ &\quad \times i^{1-\bar{l}} e^{i\delta_{\bar{\kappa}}} \left\langle \bar{a} \| Q_1^{(1)} \| a \right\rangle (-1)^{\bar{j}+j+1} \end{aligned} \tag{1}$$

In the above equation, the superscript "1" on T represents the electric transition whereas the subscripts "1" and "0" indicate respectively the order of the transition (which is dipole in the present case) and linear polarization of the photon, $\begin{pmatrix} a & b & c \\ d & e & f \end{pmatrix}$ is a $3j$ symbol, and $\left\langle \bar{a} \| Q_1^{(1)} \| a \right\rangle$ is the (complex) reduced matrix element. $\delta_{\bar{\kappa}}$ is the phase of the continuum wave with $\bar{\kappa} = \mp(\bar{j} + \frac{1}{2})$ for $\bar{j} = (\bar{l} \pm \frac{1}{2})$, and $\Omega_{\kappa m}$ is defined as

$$\begin{aligned} \Omega_{\kappa m}(\hat{n}) &= \sum_\nu \left\langle l \; m-\nu \; \frac{1}{2} \; \nu \middle| l \; \frac{1}{2} \; j \; m \right\rangle Y_{lm-\nu}(\hat{n}) \chi_\nu \\ &= \left\langle l \; m+\frac{1}{2} \; \frac{1}{2} \; -\frac{1}{2} \middle| l \; \frac{1}{2} \; j \; m \right\rangle Y_{lm+\frac{1}{2}}(\hat{n}) \chi_{-\frac{1}{2}} \\ &+ \left\langle l \; m-\frac{1}{2} \; \frac{1}{2} \; \frac{1}{2} \middle| l \; \frac{1}{2} \; j \; m \right\rangle Y_{lm-\frac{1}{2}}(\hat{n}) \chi_{\frac{1}{2}} \end{aligned} \tag{2}$$

In the above equation, $Y_{lm-\nu}(\hat{n})$ are the spherical harmonics, χ_ν is the two-component spinor weighted with the corresponding Clebsch-Gordon coefficients. The complex amplitude $T_{10}^{(1\nu)}$ consists of various terms including the angle dependent spherical harmonics. These are responsible, along with relativistic and correlation effects, for the phase, and the resulting Wigner time delay, to become angle-dependent. A shorthand notation,

$$D_{lj\to\bar{l}\bar{j}} = i^{1-\bar{l}} e^{i\delta_{\bar{\kappa}}} \left\langle \bar{a} \| Q_1^{(1)} \| a \right\rangle \ , \tag{3}$$

is used for simplicity. The present work deals with the photoionization from the spin-orbit split $3d$ subshells. There are 10 transition amplitudes due to possible transitions from the spin-orbit split $3d$ states [34]. The six transitions from the $3d_{5/2}$ subshell are listed below:

$$\begin{aligned} [T_{10}^{1+}]_{3d_{5/2}}^{m=\frac{1}{2}} &= \frac{1}{\sqrt{15}} Y_{10} D_{3d_{5/2}\to\epsilon p_{3/2}} - \frac{1}{7\sqrt{10}} Y_{30} D_{3d_{5/2}\to\epsilon f_{5/2}} \\ &\quad - \frac{\sqrt{2}}{7} Y_{30} D_{3d_{5/2}\to\epsilon f_{7/2}} \end{aligned} \tag{4a}$$

$$\begin{aligned} [T_{10}^{1-}]_{3d_{5/2}}^{m=\frac{1}{2}} &= \frac{1}{\sqrt{30}} Y_{11} D_{3d_{5/2}\to\epsilon p_{3/2}} + \frac{1}{7}\sqrt{\frac{2}{15}} Y_{31} D_{3d_{5/2}\to\epsilon f_{5/2}} \\ &\quad - \frac{1}{7}\sqrt{\frac{3}{2}} Y_{31} D_{3d_{5/2}\to\epsilon f_{7/2}} \end{aligned} \tag{4b}$$

$$\begin{aligned} [T_{10}^{1+}]_{3d_{5/2}}^{m=\frac{3}{2}} &= \frac{1}{\sqrt{15}} Y_{11} D_{3d_{5/2}\to\epsilon p_{3/2}} - \frac{1}{7}\sqrt{\frac{3}{5}} Y_{31} D_{3d_{5/2}\to\epsilon f_{5/2}} \\ &\quad - \frac{5}{14\sqrt{3}} Y_{31} D_{3d_{5/2}\to\epsilon f_{7/2}} \end{aligned} \tag{4c}$$

$$[T_{10}^{1-}]_{3d_{5/2}}^{m=\frac{3}{2}} = \frac{1}{7}\sqrt{\frac{3}{2}} Y_{32} D_{3d_{5/2}\to\epsilon f_{5/2}} - \frac{1}{14}\sqrt{\frac{10}{3}} Y_{32} D_{3d_{5/2}\to\epsilon f_{7/2}} \tag{4d}$$

$$[T_{10}^{1+}]_{3d_{5/2}}^{m=\frac{5}{2}} = -\frac{1}{7}\sqrt{\frac{5}{6}} Y_{32} D_{3d_{5/2}\to\epsilon f_{5/2}} - \frac{\sqrt{6}}{14} Y_{32} D_{3d_{5/2}\to\epsilon f_{7/2}} \tag{4e}$$

$$[T_{10}^{1-}]_{3d_{5/2}}^{m=\frac{5}{2}} = \frac{\sqrt{5}}{7} Y_{33} D_{3d_{5/2}\to\epsilon f_{5/2}} - \frac{1}{14} Y_{33} D_{3d_{5/2}\to\epsilon f_{7/2}} \tag{4f}$$

The photoionization Wigner (WES) time delay is now readily obtainable for photoionization in a given channel as

$$\tau = \hbar \frac{d\eta}{dE} \quad , \quad \eta = \tan^{-1}\left\{ \frac{\mathrm{Im}[T_{10}^{1\pm}]}{\mathrm{Re}[T_{10}^{1\pm}]} \right\} \tag{5}$$

In the following we adopt the atomic units and set $e = m = \hbar = 1$.

The subshell time delay, averaged over initial m-states, and summed over final spins of the photoelectron, is given by the weighted average

$$\bar{\tau}_{3d_{\frac{5}{2}}} = \frac{\sum_{s=+,-} \sum_{\bar{j}} \tau_{3d_{\frac{5}{2}}}^{m=\bar{j},s} \left| [T_{10}^{1\pm}]_{3d_{\frac{5}{2}}}^{m=\bar{j}} \right|^2}{\sum_{\bar{j}} \left| [T_{10}^{1\pm}]_{3d_{\frac{5}{2}}}^{m=\bar{j}} \right|^2} \tag{6}$$

B. Relativistic random phase approximation with relaxation (RRPA-R)

The radial transition matrix elements required for the calculation of the transition amplitudes, Eq (3),

are determined in the present work using the RRPA-R formalism [37]. This many-body approach considers the electron correlations and relativistic effects as in RRPA [41], but in addition it includes the effect of relaxation of the core. RRPA-R employs two sets of orbitals during the calculation; (i) ground state orbitals of the unperturbed initial state of the closed-shell target (same as in the RRPA), and (ii) orbitals of the relaxed core with a hole in the subshell from which the photoelectron originates. The potential V^{N-1}, i.e., the potential felt by the excited electron is calculated using the relaxed orbitals calculated using the self-consistent field of the ion having $N-1$ electrons and a hole in the given subshell. The Dirac-Fock orbital eigenvalues are taken as theoretical threshold values in the RRPA method, whereas the difference between the self-consistently calculated total energies of the $N-1$ electron system with a hole in specific subshells and the initial N-electron system (atom or ion),($\Delta E_{\rm SCF}$) , are used as the ionization thresholds in the RRPA-R method. The present study aims at investigating the effect of the spin-orbit interaction on the photoionization time-delay in the transition channels from the spin-orbit split 3d subshell. The SOIAIC effect emerges from interchannel coupling between the transition channels originating from the $3d_{5/2}$ and $3d_{3/2}$ subshells and modifies the uncoupled transition matrix elements. The SOIAIC effect is more pronounced in the $3d_{5/2}$ channels as compared to $3d_{3/2}$. The present work discusses results obtained at two different levels of truncation of the RRPA-R to spotlight the effects of the coupling between channels, as detailed below:

Level 1: (10 channels coupled)
$3s_{1/2} \rightarrow \epsilon p_{1/2}, \epsilon p_{3/2},$
$3p_{1/2} \rightarrow \epsilon s_{1/2},\ \epsilon d_{3/2}$
$3p_{3/2} \rightarrow \epsilon s_{1/2},\ \epsilon d_{3/2},\ \epsilon d_{5/2}$
$3d_{5/2} \rightarrow \epsilon p_{3/2},\ \epsilon f_{5/2},\ \epsilon f_{7/2}$

Level 2: (13 channels coupled)
$3s_{1/2} \rightarrow \epsilon p_{1/2}, \epsilon p_{3/2},$
$3p_{1/2} \rightarrow \epsilon s_{1/2},\ \epsilon d_{3/2}$
$3p_{3/2} \rightarrow \epsilon s_{1/2},\ \epsilon d_{3/2},\ \epsilon d_{5/2}$
$3d_{3/2} \rightarrow \epsilon p_{1/2},\ \epsilon p_{3/2},\ \epsilon f_{5/2}$
$3d_{5/2} \rightarrow \epsilon p_{3/2},\ \epsilon f_{5/2},\ \epsilon f_{7/2}$

At the 1st level of the RRPA-R, the transition channels from the $3d_{3/2}$ subshell are excluded whereas they are included in the 2nd level of truncation. Other channels which are important in the energy region studied in the present work, from the $3p$ and the $3s$ subshells, are included in both sets of calculations. As mentioned, comparison between the two sets of calculations enables us to delineate the SOIAIC effect on photoionization/photodetachment time delay.

III. RESULTS AND DISCUSSION

The primary aim of the present study is to investigate the SOIAIC effect on photoionization/photodetachment time delay along the Xe isoelectronic sequence including the Cs^+ and I^- ions.

A: Xenon atom

Partial cross sections calculated using RRPA-R for Xe $3d_{5/2}$ and Xe $3d_{3/2}$ have been reported earlier [36] but have been repeated in the present work for consistency. Studies of photoionization time delay from the $4d$ subshell of Xe have been reported [8, 29, 42], but the Xe $3d$ case which exhibits SOIAIC, has not been explored yet.

In FIG. 1, the dotted curves show the cross sections obtained using RRPA-R excluding coupling between the channels from $3d_{5/2}$ and $3d_{3/2}$subshells (level 1) whereas the solid curves show the cross section including interchannel coupling (level 2); note that for this level 2 calculation, a small region below the $3d_{3/2}$ threshold which is dominated by autoionizing resonance is omitted from the figure for clarity of presentation. The present results are obviously the same as those reported in [36], which are not shown. The difference between the coupled and uncoupled $3d_{5/2}$ cross sections due to SOIAIC is evident in the structure in the coupled cross section in the 700 eV region. Also shown in the same figure are the results of experiment [30] and earlier theoretical results from relativistic time-dependent density functional theory (RTDDFT) calculations [42]. The general agreement among the present results, experiment, and the earlier RTDDFT calculation indicate the quality of the present results; the slight overall shifts in energy result simply from the differences in threshold energies. We note that the resonances in the omitted autoionizing region are $3d_{3/2} \rightarrow np$ and nf. Both of the resonance series are rather weak, in this case. The np series is weak because the $l \rightarrow l-1$ resonances are virtually always weak [38], and the nf series is weak because the effective f-wave potential in Xe is double-welled [43]. Therefore the nf states are bound in the outer well, so that the overlap between the $3d$ and nf states is exceedingly small.

The results for the photoelectron angular asymmetry β parameter are presented in FIG. 2. Here it is seen that SOIAIC in only a very small effect. This is because the β parameter is a ratio of matrix elements [38, 39] so that the SOIAIC modification of the matrix elements, seen clearly in the cross section, largely cancels out in the β parameter. The excellent agreement of the present results with experiment and the earlier calculation indicates that not only the magnitudes of our calculated matrix elements are accurate, as indicated by the cross section, but also their phases are accurate as well. This indicates that the photoionization time delay calculated using these matrix elements are likely to be accurate as well.

The time delay in photoionization from the $3d_{5/2}$ sub-

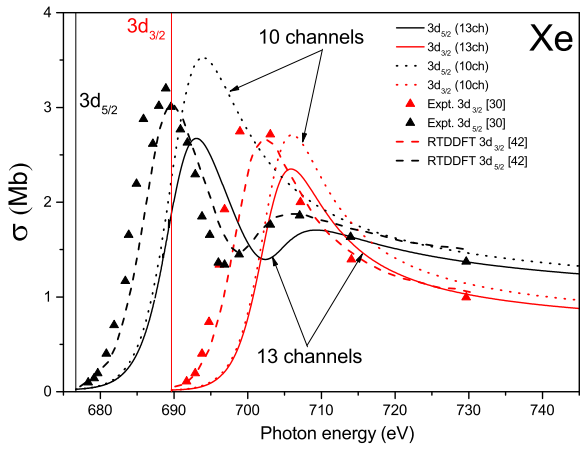

FIG. 1: (Color online) Partial cross sections for the $3d_{5/2}$ (black) and $3d_{3/2}$ (red) subshells of Xe. The solid and dotted curves are the present 13 and 10 channel RRPA-R results, respectively; the dashed curves are RTDDFT results [42], and the points are experiment [30]. The RRPA-R thresholds are indicated by vertical lines. The offset between RRPA-R and RTDDFT cross sections result from differing theoretical thresholds. The short vertical line at about 687 eV indicates the start of the resonance region.

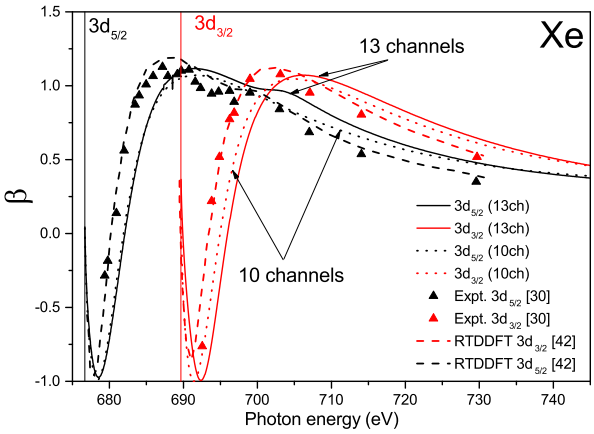

FIG. 2: (Color online) Angular asymmetry β parameters for the $3d_{5/2}$ (black) and $3d_{3/2}$ (red) subshells of Xe. The solid and dotted curves are the present 13 and 10 channel RRPA-R results, respectively; the dashed curves are RTDDFT results [42], and the points are experiment [30]. The RRPA-R thresholds are indicated by vertical lines. The offset between RRPA-R and RTDDFT cross sections result from differing theoretical thresholds. The short vertical line at about 687 eV indicates the start of the resonance region.

shell, averaged over initial m-states, and summed over final spins of the photoelectron, Eq. (6), is presented in FIG. 3. Both levels of truncation are compared to examine the SOIAIC effect. The photoionization time delay with inclusion of interchannel coupling from both the $3d_{5/2}$ and the $3d_{3/2}$ subshells exhibits a very deep minimum around 702 eV, followed by a hump, as a result of the SOIAIC. The time delay profile is qualitatively similar for all the angles; the actual numerical values are, however, different, if only slightly. Basically, the comparison of the two levels of calculation demonstrates a significant SOIAIC effect over an approximately 20 eV energy range, from about 695 eV to 715 eV. Above and below this range, however, all the curves obtained using the two different level of truncation merges together. The RRPA-R results with coupling in the small energy region (between the short vertical bar and the ionization threshold) comprising of autoionization resonances below the $3d_{3/2}$ threshold have not been shown to avoid confusion. Note also that below the region, where the SOIAIC effect is dominant, as well as in the SOIAIC region, the $3d_{5/2}$ time delay is strongly angle-dependent. This stems from the fact that the $3d_{5/2} \rightarrow \epsilon p$ and $3d_{5/2} \rightarrow \epsilon f$ matrix elements are of roughly the same magnitude in this region with each dominating at different angles, as given in Eqs. (4). At the higher energies, where $3d_{5/2} \rightarrow \epsilon f$ dominates, no such angular dependence is seen. In any case, these predictions concerning the time delay in the SOIAIC region should be looked at experimentally.

B: Cs^+ ion

In FIG. 4, the dotted curves show the cross sections obtained using RRPA-R excluding coupling between the channels from $3d_{5/2}$ and $3d_{3/2}$ subshells (level 1). The solid curves show the cross section including interchannel coupling (level 2); again the autoionizing region is omitted for clarity. The difference between the coupled and uncoupled $3d_{5/2}$ cross sections is evident from the structure in the coupled cross section in the 754 eV region. This is due to the SOIAIC effect. Also shown in the same figure are the earlier theoretical results from RTDDFT calculations [42]. Both the results are in quite good agreement; the slight overall shifts in energy result simply from the differences in threshold energies. The details of the SOIAIC structure in the $3d_{5/2}$ cross section differ significantly from the Xe case. This is due to the combined effects of differences in the matrix elements and the separation of the $3d_{5/2}$ and $3d_{3/2}$ in Cs^+ vs. Xe. Also, unlike Xe, for Cs^+ the $3d_{5/2}$ cross section has a very significant structure just below the $3d_{3/2}$ threshold when coupling between the $3d_{5/2}$ and $3d_{3/2}$ channels is included due to the resonant $3d_{3/2} \rightarrow nf$ excitations. The resonances are quite strong for Cs^+ because of the increased nuclear charge along with the increased ionicity results in the collapse of the higher nf bound states [44]. Therefore the first antinodes of the nf states reside in the inner well of the potential, thereby dramatically increasing the overlap with the $3d$ bound states in Cs^+. This phenomenon has been observed in the RTDDFT calculation [42] as well.

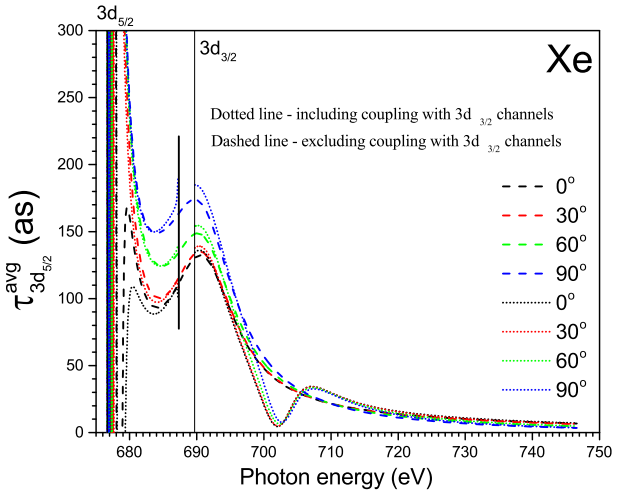

FIG. 3: (Color online) WES time delay for Xe $3d_{5/2}$ photoemission by linearly polarized photons, averaged over initial magnetic substates and photoelectron spin directions, calculated using RRPA-R with (dotted curve, 13 channels) and without (dashed curve, 13 channels) coupling with the $3d_{3/2}$ channels for 0, 30, 60 and 90 degrees angles of photoemission with respect to the photon polarization. The RRPA-R thresholds are indicated by vertical lines. The short vertical line at about 687 eV indicates the start of the resonance region.

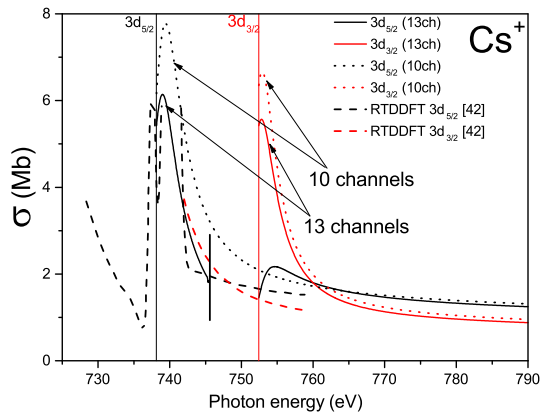

FIG. 4: (Color online) Partial cross sections for the $3d_{5/2}$ (black) and $3d_{3/2}$ (red) subshells of Cs^+. The solid and dotted curves are the present 13 and 10 channel RRPA-R results, respectively; the dashed curves are RTDDFT results [42]. The RRPA-R thresholds are indicated by vertical lines. The offset between RRPA-R and RTDDFT cross sections result from differing theoretical thresholds. The short vertical line at about 745 eV indicates the start of the resonance region.

FIG. 5 shows the angular distribution asymmetry parameter β for Cs^+. The region involving resonances has been omitted as mentioned before. Unlike the case for Xe, FIG. 2, in which the asymmetry parameter diminishes from the threshold, in the case of Cs^+, β rises from the threshold, starting from 0.6 which is close to the non-relativistic signature value [45] of β corresponding to the dominance of the $d \rightarrow f$ channels. An abrupt increase in β for the $3d$ photoionization of neutral Cs due to SOIAIC was predicted at 2 eV above the $3d_{3/2}$ threshold [46] and later seen in an experiment [47]. In the present case, due to the ionicity of Cs^+, this feature seems to have moved below the $3d_{3/2}$ threshold. Overall, however, the SOIAIC effect is small for the same reasons discussed in connection with Xe.

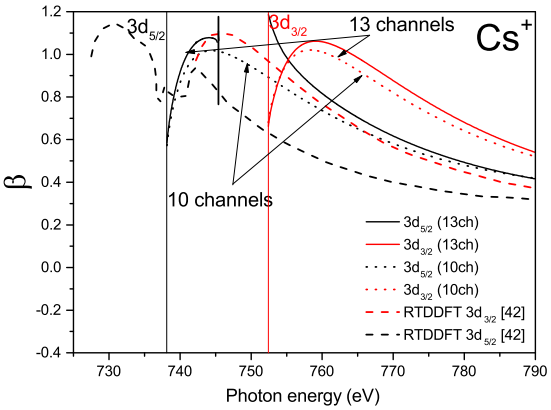

FIG. 5: (Color online) Angular asymmetry β parameters for the $3d_{5/2}$ (black) and $3d_{3/2}$ (red) subshells of Cs^+. The solid and dotted curves are the present 13 and 10 channel RRPA-R results, respectively; the dashed curves are RTDDFT results [42]. The RRPA-R thresholds are indicated by vertical lines. The offset between RRPA-R and RTDDFT cross sections result from differing theoretical thresholds. The short vertical line at about 745 eV indicates the start of the resonance region.

The time delay in photoionization from the $3d_{5/2}$ subshell of Cs^+, averaged over initial m-states, and summed over final spins of the photoelectron, Eq. (6), is presented in FIG. 6. Both the levels of truncation studied in the present work are compared to illustrate the SOIAIC effect. The photoionization time delay with inclusion of interchannel coupling between the $3d_{5/2}$ and the $3d_{3/2}$ subshells exhibits a hump around 753 eV (rather than a dip followed by a hump), as a result of the SOIAIC. The SOIAIC region is only about 10 eV wide, starting at the $3d_{3/2}$ threshold, but the deviation is very large; at its maximum, the coupling increases the time delay by more than 100 as. The profile is qualitatively similar for all the angles, thereby indicating that the $3d_{5/2} \rightarrow \epsilon f$ matrix element dominates over the whole range of energies; all the curves obtained using the two different level of truncation come together below the autoionization region and above about 762 eV. There is a very rich resonance structure in the time delay in $3d_{5/2}$ photoionization below the $3d_{3/2}$ threshold which has not been shown to avoid any confusion regarding the aim of the present study. It is

evident, however, that the SOIAIC effect on the time delay extends into the autoionizing region below the $3d_{3/2}$ threshold, but as mentioned, this region has not been investigated. In any case, however, the time delay in the region of the SOIAIC effect is ripe for experimental investigation.

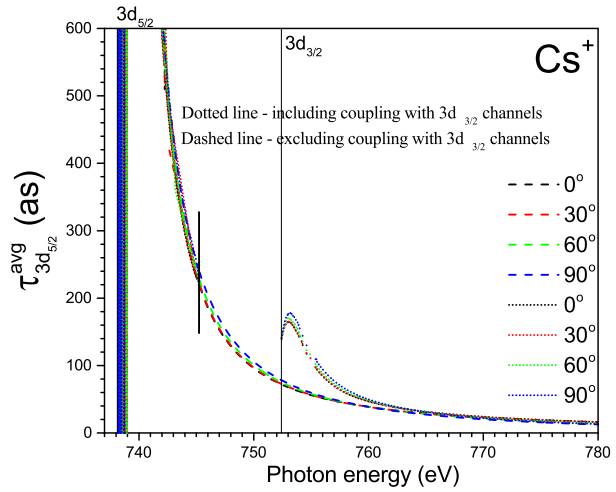

FIG. 6: (Color online) WES time delay for Cs^+ $3d_{5/2}$ photoemission by linearly polarized photons, averaged over initial magnetic substates and photoelectron spin directions, calculated using RRPA-R with (dotted curve, 13 channels) and without (dashed curve, 13 channels) coupling with the $3d_{3/2}$ channels for 0, 30, 60 and 90 degrees angles of photoemission with respect to the photon polarization. The RRPA-R thresholds are indicated by vertical lines. The short vertical line at about 745 eV indicates the start of the resonance region.

C: I^- ion

Looking now at the negative iodine ion illustrated in FIG. 7, the dotted curves show the cross sections obtained using RRPA-R excluding coupling between the channels from $3d_{5/2}$ and $3d_{3/2}$ subshells (level 1) and the solid curves show the cross section including interchannel coupling (level 2). The difference between the coupled and uncoupled $3d_{5/2}$ cross section is evident from the substantial decrease of the magnitude and a slight dip in the coupled calculation around 660 eV due to SOIAIC. But, the effect is not as pronounced as the other two cases. This phenomenology stems from the fact that, of the three cases studied, I^-, being a negative ion, has the weakest attractive potential, of the three case, for the final-state continuum electron in a photoabsorption process. Thus, the f-electron is pushed out furthest in this case, so that the maxima in the $3d \rightarrow f$ cross sections are about 30 eV above threshold, as opposed to the Xe case where they are more like 10 eV above their respective thresholds. As a consequence, in the uncoupled cross sections, the $3d_{5/2}$ cross section is larger than the $3d_{3/2}$, even at the maximum in the $3d_{5/2}$ cross section, as seen in FIG. 7, again unlike the Xe case. Thus, the interchannel effect on the $3d_{5/2}$ cross section is much weaker here, and this is seen in the coupled results in FIG. 7. In addition, the threshold behavior of the $3d$ cross sections for I^- differs from those of Xe an Cs^+ because the photodetachment cross section increases from zero at threshold, as expected from the Wigner threshold law [48]. Also shown in the same figure are the results from relativistic time-dependent density functional theory (RTDDFT) calculations [42]. Both the results are in very good agreement; the slight overall shifts in energy result simply from the differences in threshold energies.

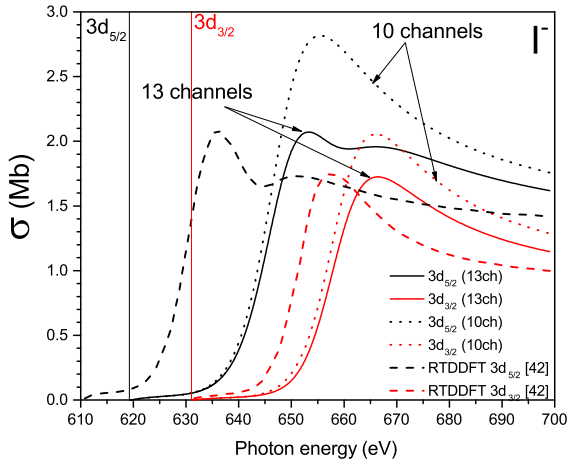

FIG. 7: (Color online) Partial cross sections for the $3d_{5/2}$ (black) and $3d_{3/2}$ (red) subshells of I^-. The solid and dotted curves are the present 13 and 10 channel RRPA-R results, respectively; the dashed curves are RTDDFT results [42]. The RRPA-R thresholds are indicated by vertical lines. The offset between RRPA-R and RTDDFT cross sections result from differing theoretical thresholds.

The angular distribution asymmetry parameter β is shown in FIG. 8 for I^- photoelectrons. The SOIAIC effect is negligible in this case since it is small in the cross section, and, owing to the nature of β as a ratio, the SOIAIC effect on the cross section are diminished, as in the previous cases. The spectral shape of the βs for I^- is similar to Xe, indicating that the phases and ratios of the magnitudes of the dipole matrix elements are not so very different in the two cases. The comparison with the RTDDFT result [42] shows excellent agreement except for the shift in energy due to differences in threshold values.

FIG. 9 shows the suitably averaged photodetachment time delay calculated at both levels of truncation. On the scale of the figure, no effect of SOIAIC is apparent. The time delay starts at a large negative value near threshold. This is characteristic of the $3d \rightarrow p$ transition which dominates near threshold as a consequence of the Wigner threshold law [48]. The time delay then increases rapidly with energy until the $3d \rightarrow f$ transitions dominate and

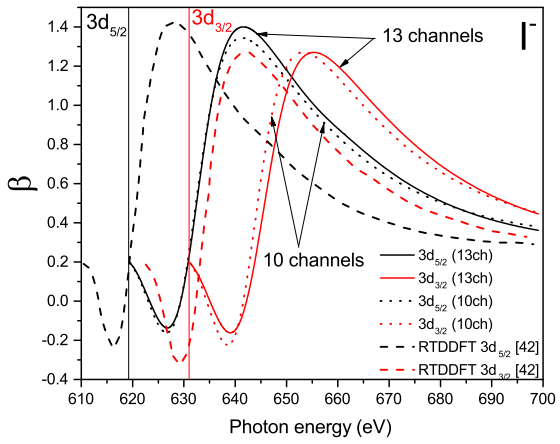

FIG. 8: (Color online) Angular asymmetry β parameters for the $3d_{5/2}$ (black) and $3d_{3/2}$ (red) subshells of I^-. The solid and dotted curves are the present 13 and 10 channel RRPA-R results, respectively; the dashed curves are RTDDFT results [42]. The RRPA-R thresholds are indicated by vertical lines. The offset between RRPA-R and RTDDFT cross sections result from differing theoretical thresholds.

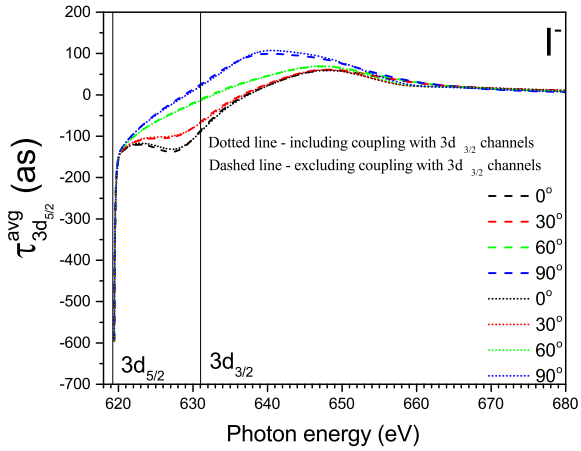

FIG. 9: (Color online) WES time delay for I^- $3d_{5/2}$ photoemission by linearly polarized photons, averaged over initial magnetic substates and photoelectron spin directions, calculated using RRPA-R with (dotted curve, 13 channels) and without (dashed curve, 13 channels) coupling with the $3d_{3/2}$ channels for 0, 30, 60 and 90 degrees angles of photoemission with respect to the photon polarization. The RRPA-R thresholds are indicated by vertical lines.

the time delay becomes positive and relatively smooth as a function of energy. Over a roughly 30 eV region, starting a bit above the threshold, the time delay shows a significant angular dependence, similar to the case of Xe and for the same reasons. Clearly the SOIAIC effect on time delay is much weaker for I^- than it was in the other two cases , just as the effect was seen to be weaker in the cross section. Looking at an expanded scale, FIG. 10, the SOIAIC effect is seen in the time delay profile around 660 eV over a 10 eV energy range, personified by a dip in the time delay. However, the effect is much smaller than in the previous two cases; for I^-, the maximum change is only about 10 as, while for Xe it was about 50 as and for Cs^+ it was about 100 as. In other words, the strength of the SOIAIC effect on time delay increases along the isoelectronic sequence. Despite the relatively small SOIAIC effect in this case, it is, nevertheless, a good candidate for measurement for two reasons: a significant angular distribution is present in the time delay over a broad energy, and, more importantly, the Coulomb laser coupling contribution is generally insignificant for photodetachment [49].

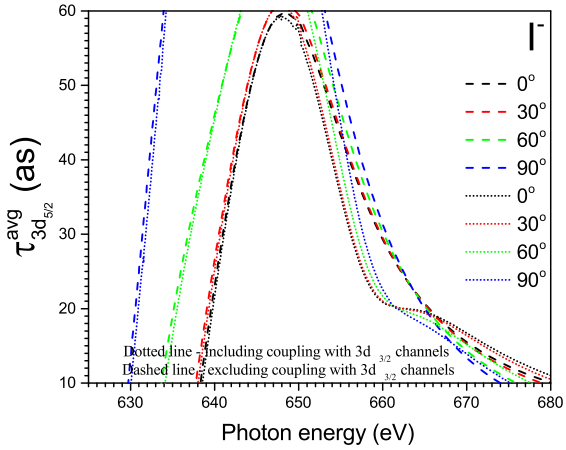

FIG. 10: (Color online) zommed in version of FIG. 9

IV. SUMMARY AND CONCLUSIONS

The spin-orbit-interaction-activated-interchannel-coupling (SOIAIC) effect on photoemission time delay has been investigated for $3d$ photoemission in the first three members of the Xe isoelectronic sequence, I^-, Xe and Cs^+. Since SOIAIC is a purely relativistic effect, brought about by the relativistic spin-orbit splitting of atomic subshells, the calculations were performed with the fully relativistic-random phase-approximation with relaxation (RRPA-R). In all three cases studied, the effects of SOIAIC show up quite strongly in the time delay, somewhat less strongly in the cross section, and least strongly in the photoelectron angular distribution β parameter. That the β parameter is least affected is owing to its nature as a ratio. The fact that the time delay is affected more than cross sections means that the interchannel coupling underpinned by the SOIAIC affects phases of matrix elements more strongly than magnitudes. In any case, this finding suggests that

SOIAIC is best studied in the time domain. It was also found that, somewhat unexpectedly, that SOIAIC become more and more important as we move from I^- to Xe and to Cs^+. This was found to be due to the details of the $3d \rightarrow f$ shape resonances relative to the splitting of the $3d$ thresholds. And this trend should continue until these resonances move below threshold into the discrete (autoionizing) region.

V. ACKNOWLEDGEMENTS

SB acknowledges the support of the Director, IIT Tirupati. The work of STM was supported by the U.S. Department of Energy, Office of Science, Basic Energy Sciences, under award DE-FG02-03ER15428.

[1] J. Itatani, F. Quéré, G. L. Yudin, M. Yu. Ivanov, F. Krausz, and P. B. Corkum, Phys. Rev. Lett. **88**, 173903 (2002).
[2] H. G. Muller, Applied Physics B **74**, s17 (2002).
[3] A. N. Pfeiffer, C. Cirelli, M. Smolarski, D. Dimitrovski, M. Abu-samha, L. B. Madsen and U. Keller, Nat. Phys. **8**, 76 (2012).
[4] M. Schultze, M. Fieβ, N. Karpowicz, J. Gagnon, M. Korbman, M. Hofstetter, S. Neppl, A. L. Cavalieri, Y. Komninos, Th. Mercouris, C. A. Nicolaides, R. Pazourek, S. Nagele, J. Feist, J. Burgdörfer, A. M. Azzeer, R. Ernstorfer, R. Kienberger, U. Kleineberg, E. Goulielmakis, F. Krausz and V. S. Yakovlev, Science **328**, 1658 (2010).
[5] K. Klunder, J. M. Dahlström, M. Gisselbrecht, T. Fordell, M. Swoboda, D. Guénot, P. Johnsson, J. Caillat, J. Mauritsson, A. Maquet, R. Taeb and A. L´ Huillier, Phys. Rev. Lett. **106**, 143002 (2011).
[6] R. Pazourek, S. Nagele, and J. Burgdörfer, Rev. Mod. Phys. **87**, 765 (2015), and references therein.
[7] T. Barillot, C. Cauchy, P. A. Hervieux, M. Gisselbrecht, S. E. Canton, P. Johnsson, J. Laksman, E. P. Mansson, J. M. Dahlström, M. Magrakvelidze, G. Dixit, M. E. Madjet, H. S. Chakraborty, E. Suraud, P. M. Dinh, P. Wopperer, K. Hansen, V. Loriot, C. Bordas, S. Sorensen, and F. Lépine, Phys. Rev. A **91**, 033413 (2015).
[8] A. S. Kheifets, S. Saha, P. C. Deshmukh, D. A. Keating, and S. T. Manson, Phys. Rev. A **92**, 063422 (2015).
[9] M. Sabbar, S. Heuser, R. Boge, M. Lucchini, T. Carette, E. Lindroth, L. Gallmann, C. Cirelli, and U. Keller, Phys. Rev. Lett. **115**, 133001 (2015).
[10] P. Hockett, E. Frumker, D. M. Villeneuve and P. B. Corkum. J. Phys. B **49**, 095602 (2016).
[11] M. Huppert, I. Jordan, D. Baykusheva, A. von Conta, and H. J. Wörner, Phys. Rev. Lett. **117**, 093001 (2016).
[12] S. Heuser, Á. Jimnez Galán, C. Cirelli, C. Marante, M. Sabbar, R. Boge, M. Lucchini, L. Gallmann, I. Ivanov A. S. Kheifets, J. M. Dahlström, E. Lindroth, L. Argenti, F. Martin and U. Keller, Phys. Rev. A **94**, 063409 (2016).
[13] V. Gruson, L. Barreau, . Jiménez-Galan, F. Risoud, J. Caillat, A. Maquet, B. Carré, F. Lepetit, J.-F. Hergott, T. Ruchon, L. Argenti, R. Taïeb, F. Martn and P. Saliéres, Science **354**, 734 (2016).
[14] M. Kotur, D. Guénot, A. Jiménez-Galn, D. Kroon, E.W. Larsen, M. Louisy, S. Bengtsson, M. Miranda, J. Mauritsson, C.L. Arnold, S.E. Canton, M. Gisselbrecht, T. Carette, J.M. Dahlström, E. Lindroth, A. Maquet, L. Argenti, F. Martin and A. L´ Huillier, Nat. Commun. **7**, 10566 (2016).
[15] A. Kheifets, A. Mandal, P. C. Deshmukh, V. K. Dolmatov, D. A. Keating, and S. T. Manson, Phys. Rev. A **94**, 013423 (2016).
[16] M. Isinger, R. J. Squibb, D. Busto, S. Zhong, A. Harth, D. Kroon, S. Nandi, C. L. Arnold, M. Miranda, J. M. Dahlstrm, E. Lindroth, R. Feifel, M. Gisselbrecht, and A. L´ Huillier, Science **358**, 893 (2017).
[17] D. A. Keating, P. C. Deshmukh and S. T. Manson, J. Phys. B **50**, 175001 (2017).
[18] L. Gallmann, I. Jordan, H. J. Wrner, L. Castiglioni, M. Hengsberger, J. Osterwalder, C. A. Arrell, M. Chergui, E. Liberatore, U. Rothlisberger and U. Keller, Struct. Dynam. **4**, 061502 (2017).
[19] M. Fanciulli, H. Volfová, S. Muff, J. Braun, H. Ebert, J. Minár, U. Heinzmann, and J. H. Dil, Phys. Rev. Lett. **118**, 067402 (2017).
[20] C. A. Nicolaides, Appl. Sci. **8**, 533 (2018).
[21] D. A. Keating, S. T. Manson, V. K. Dolmatov, A. Mandal, P. C. Deshmukh, F. Naseem, and A. S. Kheifets, Phys. Rev. A **98**, 013420 (2018).
[22] P. C. Deshmukh, A. Kumar, H. R. Varma, S. Banerjee, S. T Manson, V. K. Dolmatov and A. S. Kheifets, J. Phys. B **51**, 065008 (2018).
[23] C. Cirelli, C. Marante, S. Heuser, C. L. M. Petersson, Á. Jiménez Galán, L. Argenti, S. Zhong, D. Busto, M. Isinger, S. Nandi, S. Maclot, L. Rading, P. Johnsson, M. Gisselbrecht, M. Lucchini, L. Gallmann, J. M. Dahlstrm, E. Lindroth, A. L´ Huillier, F. Martin and U.Keller, Nat. Commun. **9**, 955 (2018).
[24] J. Vos, L. Cattaneo, S. Patchkovskii, T. Zimmermann, C. Cirelli, M. Lucchini, A. Kheifets, A. S. Landsman and U. Keller, Science **360**, 1326 (2018).
[25] E. P. Wigner, Phys. Rev. **98**, 145 (1955).
[26] L. Eisenbud, The Formal Properties of Nuclear Collisions, Ph.D. thesis, Princeton University, 1948.
[27] F. T. Smith, Phys. Rev. **118**, 349 (1960).
[28] S. Banerjee, P. C. Deshmukh, V. K. Dolmatov, S. T. Manson and A. S. Kheifets, Phys. Rev. A **99**, 013416 (2019).
[29] S. Saha, A. Mandal, J. Jose, H. R. Varma, P. C. Deshmukh, A. S. Kheifets, V. K. Dolmatov and S. T. Manson Phys. Rev. A **90**, 053406 (2014).
[30] A. Kivimäki, U. Hergenhahn, B. Kempgens, R. Hentges, M. N. Piancastelli, K. Maier, A. Ruedel, J. J. Tulkki, and A. M. Bradshaw, Phys. Rev. A **63**, 012716 (2000).
[31] M. Ya. Amusia, L. V. Chernysheva, S. T. Manson, A. M. Msezane, and V. Radojević, Phys. Rev. Lett. **88**, 093002 (2002).
[32] M. Ya. Amusia, N. A. Cherepkov, L. V. Chernysheva, Z. Felfli, and A. Z. Msezane, Phys. Rev. A **70**, 062709 (2004).
[33] S. S. Kumar, T. Banerjee, P. C. Deshmukh and S. T.

Manson, Phys. Rev. A **79**, 043401 (2009).
[34] A. Mandal, P. C. Deshmukh, A. S. Kheifets, V. K. Dolmatov, and S. T. Manson, Phys. Rev. A **96**, 053407 (2017).
[35] A. Mandal et al., Springer Proceedings of ISAMP TC-7 (2018).
[36] V. Radojević, D. M. Davidović, and M. Ya. Amusia, Phys. Rev. A **67**, 022719 (2003).
[37] V. Radojević, M. Kutzner and H. P. Kelly, Phys. Rev. A **40**, 727 (1989).
[38] A. F. Starace, in Handbuch der Physik, Vol. 31, edited by W. Mehlhorn (Springer, Berlin, 1982), pp. 1-121.
[39] S. T. Manson and A. F. Starace, Rev. Mod. Phys. **54**, 389 (1982).
[40] J. Wätzel, A. S. Moskalenko, Y. Pavlyukh and J. Berakdar, J. Phys. B **48**, 025602 (2015).
[41] W. R. Johnson and C. D. Lin Phys. Rev. A **20**, 964 (1979).
[42] D. Toffoli, M. Stener, and P. Decleva, J. Phys. B **36**, 3097 (2003).
[43] A. R. P. Rau and U. Fano, Phys Rev. **167**, 7 (1968).
[44] K.T. Cheng and C. Froese Fischer, Phys. Rev. A **28**, 2811 (1983).
[45] J. Cooper and R.N. Zare, J. Chem. Phys. **48**, 942-943 (1968).
[46] M. Ya. Amusia, A. S. Baltenkov, L. V. Chernysheva, Z. Felfli, S. T. Manson and A. Z. Msezane, J. Phys. B **37**, 937 (2004).
[47] T. Richter, E. Heinecke, P. Zimmermann, K. Godehusen, M. Yalinkaya, D. Cubaynes, and M. Meyer, Phys. Rev. Lett. **98**, 143002 (2007).
[48] E. P. Wigner, Phys. Rev. **73**, 1002 (1948).
[49] E. Lindroth and J. M. Dahlström, Phys. Rev. A **96**, 013420 (2017).
[50] I. Jordan, M. Huppert, S. Pabst, A. S. Kheifets, D. Baykusheva and H. J. Wörner, Phys. Rev. A **95**, 013404 (2017).